Sustainable Energy Research

RESEARCH

Open Access

# Development of a portable small wind turbine for integration into a mobile cooling technology

Perm Mthethwa[1*], Tilahun S. Workneh[2] and Alaika Kassim[2]

## Abstract

In this study, a small wind turbine prototype was developed to provide electric power for a mobile cooling unit The aim of this study was to design and develop a 600-W small wind turbine that can generate electric energy to power a mobile cooling unit used for the storage of fruits and vegetables, mainly for the benefit of smallholder farmers. Smallholder farmers suffer from high postharvest losses, approximated at 50%, some of which can be avoided by using efficient low-cost cooling units, rather than open transport. Cooling slows down the metabolic rate which consequently extends the produce's shelf life and prevents spoilage, allowing farmers to provide high-quality produce to the market. This could potentially increase the farmers' monetary returns. The study was conducted in KwaZulu-Natal on the road that stretches between Pietermaritzburg and Estcourt. The wind turbine is made of a 600-mm-diameter rotor with three PVC blades, a permanent magnet synchronous generator, a bridge rectifier, a 230-V AC inverter and a battery for energy storage. The wind turbine was tested against three vehicle speeds of 60, 80, and 100 km $h^{-1}$, and the two opening levels, level 1 at 45° and level 2 at 80° relative to the louvre mechanism frame. The results of this study revealed that the power generated by the wind turbine is greatly influenced ($p < 0.001$) by both the vehicle travelling speed and louvre opening level. The power output of 113.4, 159.6 and 210.0 W per hour was observed for the vehicle speeds of 60, 80 and 100 km $h^{-1}$, respectively, on louvre opening level 1. The power output of 142.8 W $h^{-1}$, 268.8 W $h^{-1}$ and 294.0 W $h^{-1}$ were observed for a wind speed of 60 km $h^{-1}$, 80 km $h^{-1}$, and 100 km $h^{-1}$, respectively, on Louvre opening level 2. This shows that higher wind speeds (vehicle speeds) produce high-power output which accounts for the small size of the wind turbine rotor. A maximum power coefficient of 0.49 was achieved for this study. The wind turbine can generate the power required to run a cooling technology to a limited extent, thus must have a backup power supply from the diesel engine or be used in a hybrid system.

**Keywords** Small wind turbine, Wind energy, Horizontal axis wind turbine, PVC blades, Postharvest losses, Mobile cooling unit, Smallholder farmers

## Introduction

Smallholder farmers experience high postharvest losses (PHLs) along the supply chain. These are estimated around 50% of the total fresh produce harvested and 23% of these losses are credited to the transportation period (Elik et al., 2019). While factors such as improper handling and significant low chill temperature may contribute to high PHL, some of these losses are as a result of the use of open space trucks and bakkies to transport fruit and vegetables (FV) by smallholder farmers. This form of

*Correspondence:
Perm Mthethwa
mthethwap@arc.agric.za
[1] Institute of Agricultural Engineering, Agricultural Research Council, Pretoria 0184, South Africa
[2] Bioresources Engineering, School of Engineering, University of KwaZulu-Natal, Pietermaritzburg 3209, South Africa

open transport is susceptible to unfavourable and uncontrolled ambient conditions that can negatively affect the FVs (Sibanda & Workneh, 2020a, 2020b). Exposure of FVs to high temperatures accelerates the ripening process which are then easily prone to spoilage (Cherono & Workneh, 2020). This exposure may not have an immediate effect during transportation, but it plays a direct role in the rapid decay of the FV in the supply chain (Mansuri et al., 2016). As a result of these PHLs, farmers make a limited profit on the revenue generated from the produce sold while some make a loss (Elik et al., 2019; Murthy et al., 2009).

Refrigerated trucks or reefer units exist which can store and transport the fruits and vegetables at optimum temperatures. Since different fresh produce are sensitive to certain temperature ranges, it is important to know the specific temperature range at which the produce variety is stored at in order to avoid it spoiling due to low freezing temperatures which affect their quality (Dew et al., 2014). Cooling offers a conventional way to extend the lifespan of FV (Sibanda & Workneh, 2020a, 2020b). Refrigerated trucks are powered by diesel fuel to run their refrigeration units, but these are cost-intensive and harmful to the environment (Sibanda & Workneh, 2020b). One of the attempts to reduce costs associated with the purchase or hire of refrigeration units is to reduce the running costs for fuel which adopts the use of an alternative, free, replenishable energy source. Power generation from renewable energy sources has gained momentum globally since the use of fossil fuels has become less appealing to the public due to its detrimental effects on the atmosphere, such as extreme, unpredictable climate change (Panja & Ganguly, 2019). The transition from fossil fuels to renewable energy sources is also driven by the debilitating availability of fossil fuels (Ozgener, 2006).

The truck transportation sector, in general, has also started the intervention to look for alternative low-cost, non-destructive energy sources to drive and power its systems at large. In an attempt to intervene in the energy crisis, some refrigerated trucks or reefer units have adopted the hybrid system of fossil fuel and solar panels as their energy source, while others use biogas. Whereas in the past solar panels were viewed as unattractive due to their high costs versus low diesel pricing, the situation has changed and solar panel pricing has been reduced to reasonable and affordable prices, which now makes it a viable option as a renewable energy source (Elik et al., 2019). Since then, the drop in the price of solar panels has been estimated to be more than 80% of the initial market price some couple of years ago. Rossetti et al. (2022) conducted a study on the implementation of a solar-aided refrigeration unit as a solution to carbon emission which influence climate change as well as the declining availability of fossil fuels. The study achieved good results with the solar panel system being able to provide 65–112% of the energy consumed by the refrigeration unit depending on the time of the day. As of 2022, South Africa's Shoprite group was reported to have 1041 trailers with solar-powered refrigeration units amongst its fleet (Kuhudzai, 2022).

Though refrigerated trucks or reefer units are a well-developed mobile cooling technology, they are still out of reach for small-scale farmers because they are costly and most smallholder farmers stay in remote rural areas which are far away from where they can easily access this type of technology for hire (Elik et al., 2019; Louw & Jordaan, 2016). Thus, the need for interference with regard to energy supply, other than solar energy. Second to solar energy, wind energy is one of the fastest growing renewable energy (Akbari et al., 2022). This is because wind energy is an abundant energy source with reasonable investment costs (Hirahara et al., 2005).

Studies have shown that all mobile reefer units require high-energy input (Telle et al., 2022; Van Duin et al., 2018). For vehicles, wind energy is one of the feasible options for electrical power generation and supply since moving vehicles give rise or create high wind speeds when the vehicle is in motion (Hossain, 2020). Generally, because large wind turbines have larger rotor areas and a gearbox, they can operate at low wind speeds (Muhsen et al., 2019; Ozgener, 2006). In the case of vehicles where there is limited space that the wind turbine can occupy, the rotor diameter is also limited, therefore the wind speed has to be optimised as much as possible to obtain the required power output.

Small wind turbines can be defined as turbines which can produce less than 50 kW of power associated with a rotor diameter of 8 m or less (Evans et al., 2018; Wood, 2011). The wind turbine captures the wind energy using the rotor blades (Shoaib et al., 2019. The rotation of the rotor causes the mechanical movement of the generator shaft which feeds the electrical generator and produces electrical energy (Chong et al., 2021). The electrical generator outputs is in the form of alternating current (AC) power which is converted into direct current (DC) power by the rectifier so that it can be stored in a battery (Shoaib et al., 2019). Since most appliances and equipment use AC power, an inverter is then used to convert power from DC to AC (Chong et al., 2021).

For the design of the rotor blade, It is important to take note of the material used to make the blades of the wind turbine since it affects the overall power output and efficiency of the system (Garmode et al., 2022). An ideal material for wind turbine blades is a material that is lightweight, resistant to heat or solar radiation exposure and has high tensile strength. Usually, glass and carbon fibre

materials are used to make the rotor blades, but these are expensive and raise the costs of a wind turbine in addition to the electrical generator costs (Garmode et al., 2022). In order to lower the costs of the wind turbine, an alternative material was found, polyvinyl chloride (PVC) pipe. A common PVC pipe used for water systems can be used as a material for wind turbine blades when cut to the right shape (Wahyudi et al., 2022). PVC pipe material is a relatively cheap, lightweight and durable material to use for small wind turbines even though its performance is less than that of conventional blade materials such as epoxy, polyester, carbon and glass fibre-reinforced polymer (Ceruti, 2019; Garmode et al., 2022).

With regard to generators used in wind turbines, recent studies show that the focus of electrical generators has shifted from fixed wind speed generators to adopting variable wind speed generators (Bracco & Razzetti, 2022; Chong et al., 2021). This is of great advantage since the apparent wind speed varies greatly and this signifies that power can be harnessed at different wind speeds and there will be a continuous power supply at all wind speeds. The doubly fed induction generator (DFIG) and permanent magnet synchronous generator (PMSG) are some of the most known and used variable wind speed electrical generators (Chong et al., 2021; Saidi et al., 2018). Unlike the DFIG, the PMSG is a direct drive generator, which eliminates the need for a gearbox for small wind turbines (Zhang et al., 2021). The PMSG outputs a three-phase alternating current (Zhang et al., 2021). Literature reveals no evidence of small wind turbines being used to harness wind energy to act as a power supply for trucks or any mobile cooling technologies while in transit. Even though research on small wind turbines being implemented on small vehicles to replace combustion engines is drawing great attention, no research is present on cooling technologies using wind turbines. The aim of this study is to design and develop a small wind turbine to power an evaporative cooler unit during the transportation of fruit and vegetables in KwaZulu-Natal.

The subject for this study is an evaporative cooler unit at Ukulinga research farm at the University of KwaZulu-Natal which serves as a guide for the amount of electrical energy that one needs to design for. The small wind turbine is designed to provide power to run this evaporative cooler. Sibanda and Workneh (2020a) designed and developed an evaporative cooler for smallholder farmers. This unit requires less energy input than that required by refrigerated units. For the purpose of research and powering a basic evaporative cooling system, only the water pump used for water circulation, the suction fans used to draw hot ambient air in from outside and another to pull cooled air inside the storage chamber, and lights were accounted for. In total, this cooling unit consumes approximately 503 W of energy per hour excluding the heat exchanger which is an enhancement for more cooling effect. The evaporative cooler also has a relatively low initial capital investment than other cooling technologies which makes it a simple and affordable cooling technology for smallholder farmers. Thus, the purpose of this study is to design, construct, test and evaluate the performance of a 600 W small wind turbine prototype, designed to power a mobile evaporative cooler unit.

## Analysis of the prototype design

The study was conducted at the University of KwaZulu-Natal (UKZN), Pietermaritzburg (PMB) Life Sciences campus, KwaZulu-Natal, South Africa. PMB has a minimum wind speed of 0.30 km $h^{-1}$ in the month of April, a maximum wind speed of 26.60 km $h^{-1}$ in the month of October and an average wind speed of 8.12 km $h^{-1}$ throughout the year. The wind turbine experimentation was conducted at Ukulinga Research Farm and on the road between PMB and Estcourt with the wind turbine mounted on a bakkie travelling at vehicle speed ranging between 60 and 100 km $h^{-1}$.

### Description of the small wind turbine

The small wind turbine design consists of the following main components: (a) a permanent magnet synchronous generator (PMSG), (b) a rotor, (c) a bridge rectifier, (d) a power inverter, (e) a lead-acid battery, (f) a supporting tower, (g) an outer protective casing, and (h) a movable louvre mechanism (Fig. 1). Figure 1 shows the overall wind turbine design with a protective casing, and then the components of the wind turbine are labelled in Fig. 2. The yaw or furling mechanism is excluded in this wind turbine design since the airflow for a vehicle in motion travels in one direction, and there is no need for the rotation of the rotor to harness wind energy. The rotor of the wind turbine remains in a fixed position throughout its operation. The protective casing as shown in Fig. 2 is an $800 \times 800 \times 500$ mm square angle steel box with an adjustable pine wood louvre mechanism for airflow control at the front and no coverage at the back. The louvre mechanism, at the front of the protective casing is used to reduce or increase incoming wind speed as required. A three-layer vanishing coat was used to protect the wood against swelling as a result of water infiltration.

The wind turbine design consists of a 600-mm rotor with three 275-mm-long blades made of PVC pipe material connected by a $15 \times 50$ mm steel metal both welded and bolted to a 60-mm-diameter circular steel metal. Due to limited space at the top of a bakkie and the general small size of farmers' bakkie, the rotor diameter was limited to 600 mm. Although the rotor size is small, the blades were optimised and designed to

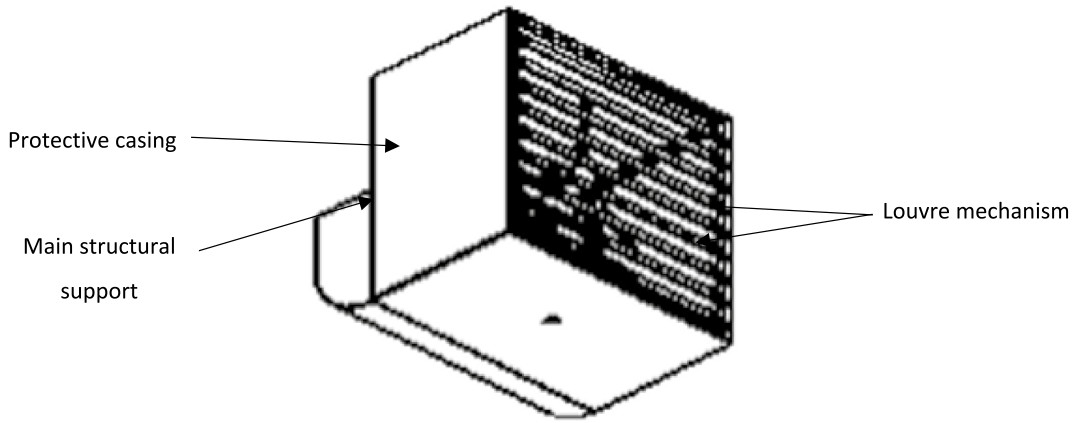


**Fig. 1** Small wind turbine design

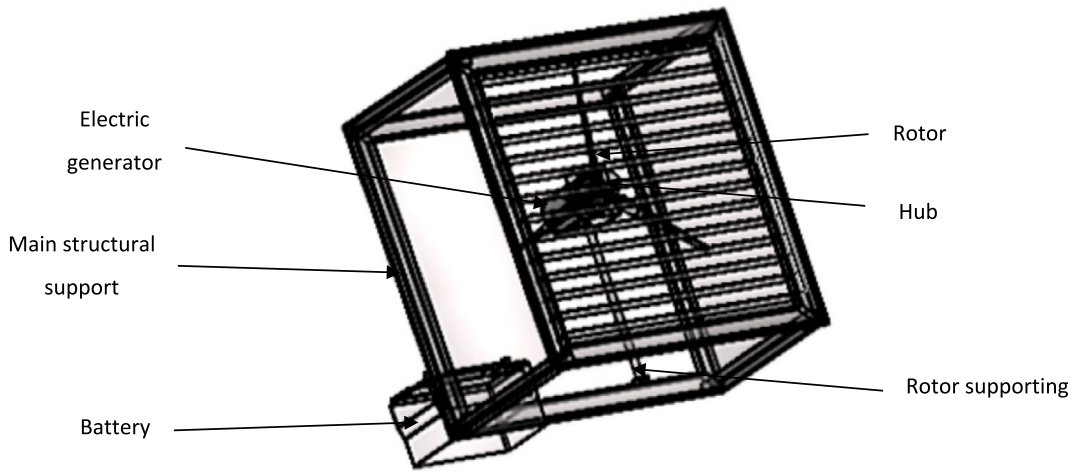


**Fig. 2** Annotated small wind turbine design

**Table 1** Chord length for different sections of the PVC pipe blade length

| Section no | *r* (m) | *c* (m) |
|---|---|---|
| 1 | 0.05 | 0.1440 |
| 2 | 0.1 | 0.1017 |
| 3 | 0.15 | 0.0738 |
| 4 | 0.2 | 0.0573 |
| 5 | 0.25 | 0.0465 |
| 6 | 0.275 | 0.0390 |

account for the small rotor size, with the anticipation that the high wind speed would make up for the small size of the rotor. The PVC blades used were heated, flattened and shaped on one side at an angle of 7° to be receptive to the incoming wind. Table 1 documents the chord lengths for each section of the PVC pipe blades as computed via the blade element momentum (BEM) theory. The PVC blades are lightweight and can withstand potential heat deformation from solar radiation on their own in addition to being shielded by the protective outer structure. The rotor is coupled directly to the PMSG via a small stainless-steel shaft of the electric generator. The wind blows on the louvre mechanism, which can lower the wind speed to a tolerable wind speed range of choice. The louvre mechanism has two opening levels. Opening levels 1 and 2 have their slats positioned at 45° and 80° angles, respectively, relative to the main support of the louvre mechanism. Isolated tests were conducted on the louvre mechanism to assess the change of wind speed at different opening angles, from 0 to 90° using the vacuum blower. The results showed that between 0–40° and 45–85°, there were no significant differences in the wind speed

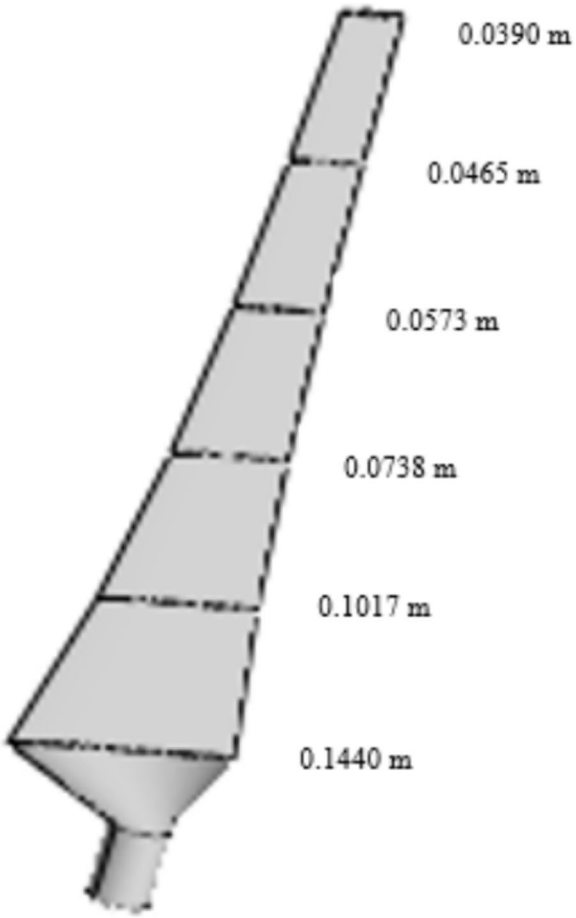


**Fig. 3** Rotor blade design with dimensioned chord lengths for each sector

reading. Thus settling for the chosen angles. At an angle greater than 90°, which is at a right angle to the frame of the louvre mechanism, the slats become a barrier and intercept the incoming wind. When the wind hits the rotor, it causes the mechanical rotation of the blades and, consequently, the coupled generator shaft (Fig. 3).

Figure 4 shows the wind turbine rotor and hub design. The PMSG then converts the mechanical energy into a three-phase alternating current (AC) electrical power. The three-phase AC power is then converted into direct current (DC) power through the bridge rectifier. This power is stored and utilised through the battery. The power inverter is used to convert DC to AC power after the battery and most importantly step-up the voltage from 12 to 230 V that can be utilised by evaporative cooling system (ECS) unit electric components. The rectifier and power inverter are connected via the battery terminals. A 12 V 105 Ah lead–acid battery was used to store and supply power for the evaporative cooler unit. Figure 5 shows the overall wind energy conversion system of the small wind turbine from wind to electrical energy. Figures 6 and 7 show the design of a portable evaporative cooler unit powered by a small wind turbine that can be loaded on the back of a bakkie or made into a trailer.

The aerodynamic wind power output equation was the main equation used to analyse the power output of the wind turbine generator as given by Eq. (1) (Schubel and Crossley, 2012; Bisoyi et al., 2013). This being the principal equation which suggests that the wind speed, with a fixed rotor diameter, can be manipulated to produce more power output, which is what this study seeks to explore. Equation (1) along with the blade element

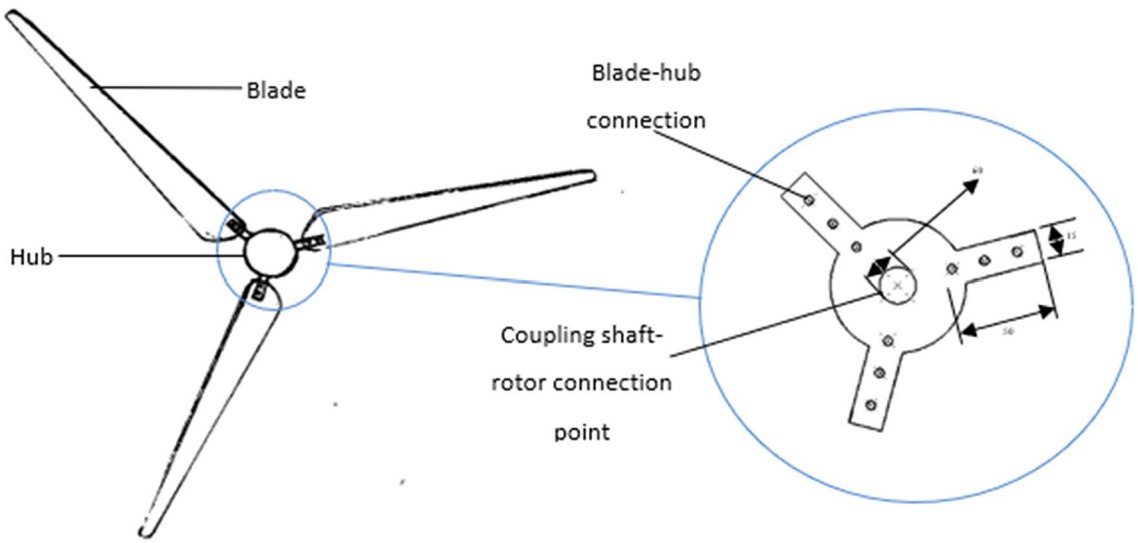


**Fig. 4** Wind turbine blades made of PVC material with a magnified hub design

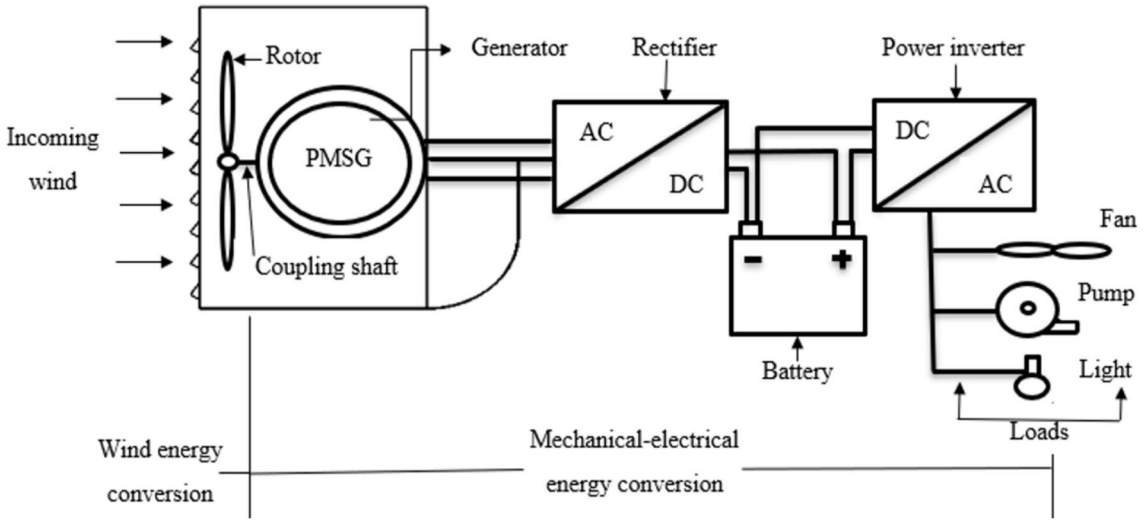


**Fig. 5** Energy conversion system of the small wind turbine

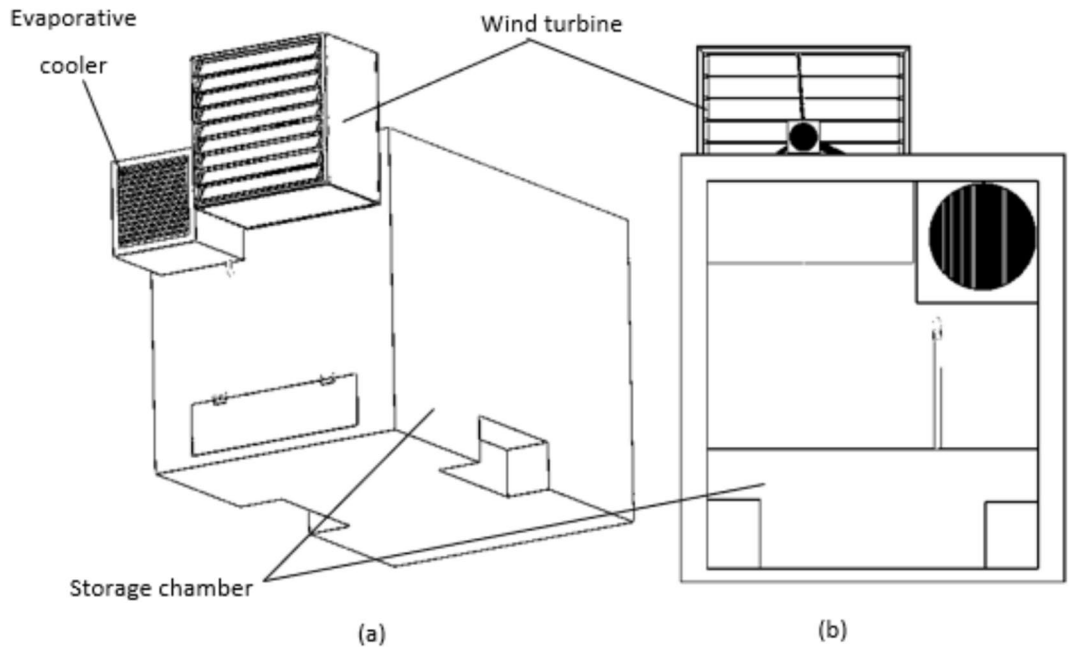


**Fig. 6** **a** Isometric view and **b** the inside of the designed portable evaporative cooler unit powered by a small wind turbine

momentum (BEM) theory and QBlade simulation were used to do the necessary computations:

$$P_T = \frac{1}{2} C_p(\lambda, \beta) \rho A V^3, \tag{1}$$

where $P_T$ stands for the aerodynamic power output (W), $C_p$ is the power coefficient, $\lambda$ is the tip speed ratio, $\beta$ is the pitch angle (°), $\rho$ is the air density (kg $m^{-3}$), A is the swept area ($m^2$), and $V_1$ is the undisturbed windspeed (m $s^{-1}$). Equation (2) was used to compute the chord lengths of the SWT blades:

$$c = \frac{16\pi r}{B(C_L)_D} \sin^2\left(\frac{1}{3}\tan^{-1}\left(\frac{R}{r\lambda_D}\right)\right), \tag{2}$$

where $c$ is the chord length, $r$ is the radial distance from the hub to the blade element (m), $B$ is the number of blades, $R$ is the radius of the rotor/blade length (m), $(C_L)_D$ is the design lift coefficient, and $\lambda_D$ is the design

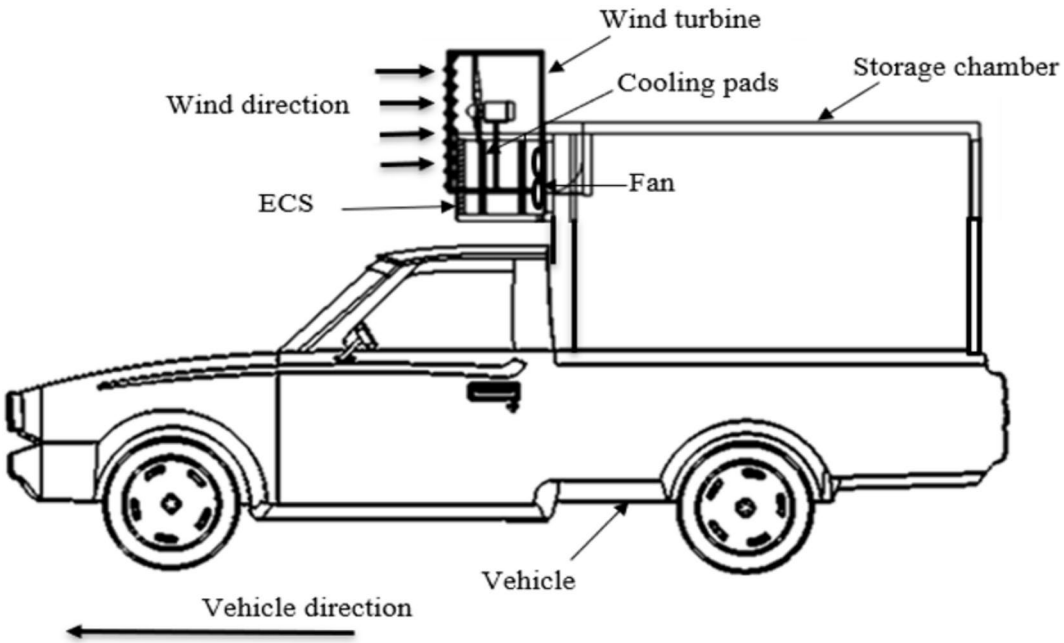


**Fig. 7** Side view of an ECS unit powered by a wind turbine mounted on a bakkie

tip speed ratio of the chord lengths presented in Table 1 are three times the original chord lengths computed from the BEM theory. QBlade was used to simulate and optimise the blade design. From QBlade it was observed that the original chord lengths did not generate the desired power outputs. Different chord lengths were tested and it was observed that at 3×of the original chord lengths, the desired power output was observed. The twist angles were generated by QBlade. Figure 3 shows the rotor blade design developed by QBlade with dimensioned chord lengths for each blade sector. The rest of the equations on the BEM theory used to compute the other design parameters (axial and tangential induction factors, inflow angle, normal and tangential loads coefficient, angle of attack, power coefficient) and the chord length are presented in the book chapter by Mthethwa et al. (2023), while the data on the design and optimisation of the blade by QBlade and Simulink are presented by Mthethwa et al. (2022).

Whilst the total power requirement of the evaporative cooling system was 503 W, an additional 15% (75.45 W) of power was accounted for in the case of power losses through the wires, rectifier and so on. The BEM theory was used to design the blades in detail. Therefore, the total power requirement of the system is 600 W. Although the ideal generator rotational speed computed using the BEM theory was around 3200 rev $min^{-1}$, the highest rotational speed generator that was found at a reasonable price in the market was 600 rpm, with the same power output of 600 W. In order to accommodate for any shortages that may arise during travel, a battery that can accommodate a two-hour travel without refilling (Equation (3):

$$\begin{aligned} P_{tot} &= P_A \times t \\ &= 600 \times 2 \\ &= 1200\ \text{Wh}, \end{aligned} \tag{3}$$

where $P_{tot}$ is the total power of the battery (Wh), $P_A$ is the aerodynamic power output (W), and $t$ is the travel duration (h). Ohm's law equation was used to determine the current rating needed to size the battery to give the required power storage as presented by Eq. (4). The required current rating of the battery was computed at 100 Ah:

$$\begin{aligned} P_{tot} &= V \times I \\ 1200 &= 12 \times I \\ I &= 100\ \text{Ah}. \end{aligned} \tag{4}$$

#### *Experimental design of the wind turbine*

The wind turbine experimental design was performed for two opening levels of the louvre mechanism and three vehicle travelling speeds as shown in Fig. 8. The purpose of this design was to explore and investigate the amount of power generated by the wind turbine at different apparent wind speeds and louvre opening levels. This is because different wind speeds generate different

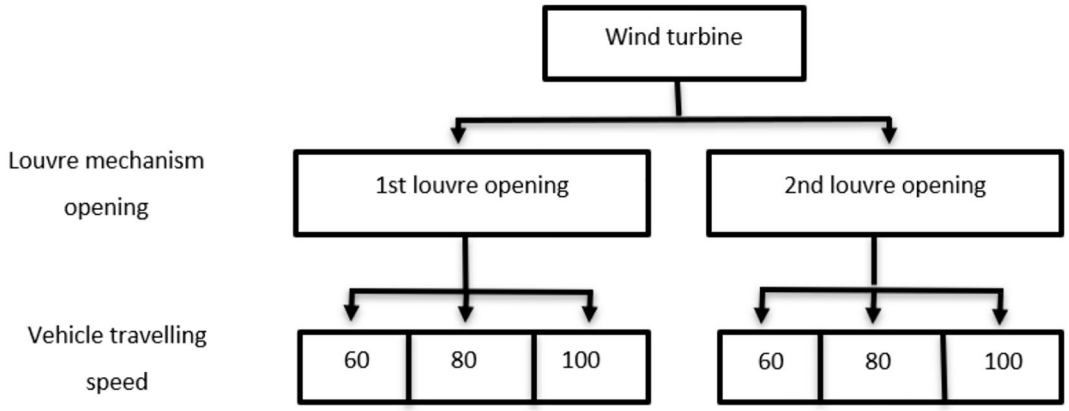


**Fig. 8** Experimental design to determine the accumulated power output of a wind turbine

power outputs and sometimes the incoming wind speed on the road can be harsh and high for the operation of the rotor and therefore the need to adjust the wind speed to the optimum wind speed range via the louvre mechanism. Thus, the need to test for different wind speeds and louvre opening levels. The BEM theory, QBlade and Matlab Simulink simulations were used to design the blades and overall wind turbine design. The testing was done for three weeks with three replications. For testing purposes, the wind turbine was mounted on the vehicle through a steel support stand as shown in Fig. 9.

The independent variable in this study was the wind speed, and the dependent variable was the power output. The pitch angle, rotor diameter, air density and TSR are the fixed variables. Since the incoming wind in a moving vehicle is in one direction and for simplicity of the design, the pitch angle is fixed at 7°, while the angle of attack may vary a bit depending on the inflow angle. The power coefficient and power output from the wind turbine were used to assess the performance of the wind turbine. Figure 9 shows the small wind turbine prototype mounted on a bakkie for testing purposes. Tables 2, 3 and 4 show the generator specifications, the rotor specifications, and the technical specifications of the wind turbine.

#### *Determination of the wind speed*

The formula used to compute the apparent wind speed generated by a moving vehicle and experienced by a stationary object on the road is represented by Eq. (5):

$$A = \sqrt{W^2 + V^2 + 2WV\cos\alpha}, \tag{5}$$

where $A$ is the apparent wind speed (m $s^{-1}$), $V$ is the vehicle speed (m $s^{-1}$), W is the true wind velocity and is the pointing angle (°) (upwind = 0 ° and downwind = 180 °).

#### *Determination of the power output*

The voltage and current of the wind turbine were measured via a multi-meter at the battery terminals. The power output is then determined through the voltage and charge capacity of the lead–acid battery as shown in Eq. (6):

$$P_A = CC \times E, \tag{6}$$

where $P_A$ is the accumulated/ aerodynamic power (Wh), CC is the capacity charge (%), and E is the electrical energy of the battery (Wh).

#### *Determination of the power coefficient*

The power coefficient was determined from the accumulated power obtained from the wind turbine testing. The rated power output of the wind turbine and the power coefficient were then used to assess the performance of the wind turbine as shown in Eq. (7):

$$C_p = \frac{P_A}{P_T}, \tag{7}$$

where $C_p$ is the power coefficient, $P_A$ is the accumulated/ aerodynamic power (Wh), and $P_T$ is the total power rating of the wind turbine (Wh).

### Data collection and analysis

The wind speed data were collected using an anemometer while the DC voltage was measured through the battery after the rectifier. GenStat software was used for the statistical analysis of the data with a 95% confidence level. The graphs used for the analysis of the results were generated by Microsoft Office Excel spreadsheet (2016). Data on the incoming wind speed at different louvre opening levels and the voltage increase in the

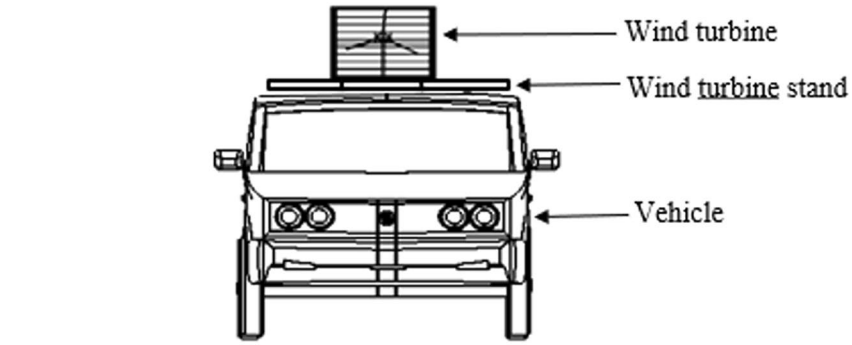


**Front view**

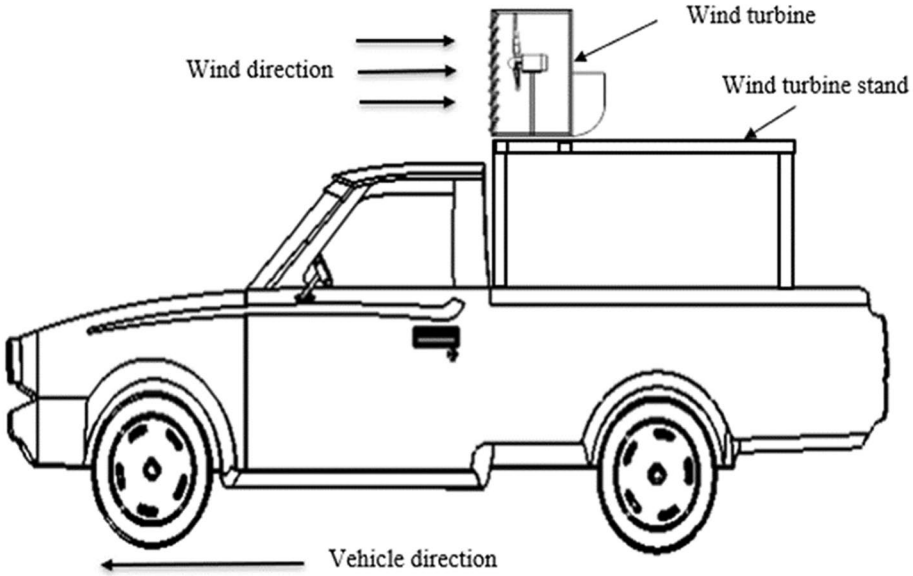


**Side view**

**Fig. 9** Small wind turbine prototype mounted on a bakkie

battery due to the wind turbine were observed. The voltage was then used to calculate the power generated by the wind turbine through capacity charge estimation. The testing was done over three weeks with three replications.

## Results and discussion

### Incoming wind speed determination

Wind speed is a fundamental parameter in the operation of a wind turbine. In this study, the operating wind speed is the apparent wind speed generated by a moving vehicle which is influenced by the daily wind speed and vehicle travelling speed. Therefore, it is important to establish the relationship between the daily wind speed, the vehicle speed and the apparent incoming wind speed. Direct wind speed measurements were made and validated against theoretical wind speed calculations.

The direct wind speed measurement data were recorded based on the incoming airflow on the road at three different travelling vehicle speeds: 60, 80 and 100 $km.h^{-1}$. The collected wind speed serves as the undisturbed wind speed from which the wind energy is harnessed. The apparent wind speed data are presented in Table 5. The apparent wind speed varies along the road for a constant vehicle travelling speed. Thus, a range of values is presented instead of a single value for

**Table 2** Generator specifications

| Parameter | Value | Units |
|---|---|---|
| Rated power | 600 | W |
| Max power | 636 | W |
| Rated voltage | 12 | V |
| Rated current | AC | – |
| Rated rotational speed | 600 | rev $min^{-1}$ |
| Top net weight | 9.0 | kg |
| Generator type | Three-phase permanent magnet synchronous generator | – |
| Shaft material | Stainless steel | – |
| Shell material | Cast iron | – |
| Protective grade | IP54 | – |
| Working temperature | −40 – +80 | °C |

**Table 3** Rotor specifications

| Parameter | Value | Units |
|---|---|---|
| Rotor diameter | 0.6 | M |
| Blade length | 0.275 | M |
| Hub | 60 | M |
| Pitch angle | 7 | ° |
| Design wind speed | 16.8 | M $s^{-1}$ |
| Tip speed ratio (TSR) | 6 | – |

**Table 4** Technical specification of the turbine

| Parameter | Value | Units |
|---|---|---|
| Nominal power output | 600 | W |
| Start-up wind speed | 4 | m $s^{-1}$ |
| Rated wind speed | 17.5 | m $s^{-1}$ |
| Survival wind speed | 33 | m $s^{-1}$ |
| Rotor diameter | 0.6 | M |
| Rotor rotational speed | 600 | rev $min^{-1}$ |
| No. of blades | 3 | – |
| Generator type | 3-phase permanent magnet synchronous generator | |
| Transmission | Gearless direct drive | |
| Output type | 230 VAC | V |

**Table 5** Wind speed data collection from a moving vehicle at different vehicle travelling speeds

| Wind speed (m $s^{-1}$) | Vehicle travelling speed (km $h^{-1}$) | Vehicle travelling speed (m $s^{-1}$) | Undisturbed/ apparent wind speed (m $s^{-1}$) |
|---|---|---|---|
| 0.8 | 60 | 16.67 | 12–14 |
| 0.8 | 80 | 22.22 | 18–27 |
| 0.8 | 100 | 27.78 | 24–29 |

**Table 6** Theoretic apparent wind speed

| Vehicle travelling speed (km $h^{-1}$) | Vehicle travelling speed (m $s^{-1}$) | Apparent wind speed (m $s^{-1}$) |
|---|---|---|
| 60 | 16.667 | 18.611 |
| 80 | 22.222 | 24.166 |
| 100 | 27.778 | 29.722 |

each vehicle's travelling speed. The apparent wind speed ranges between 12 and 14 m $s^{-1}$ for a vehicle speed of 60 km $h^{-1}$, 18–27 m $s^{-1}$ for a vehicle speed of 80 km $h^{-1}$ and 24–29 m $s^{-1}$ for a vehicle speed of 100 km $h^{-1}$. According to these findings, the apparent wind speed is directly and closely dependent on the vehicle's travelling speed although it is not exact. This may be due to wind fluctuations associated with the change in topography and terrain which act as obstructions along the road. A downward slope will cause an increase in airflow downhill while going uphill will reduce the airflow. The airflow is high in low-lying terrains and elevated regions while it is low in high-rising terrains and depressed regions. This wind speed data collection was carried out in Pietermaritzburg which is characterised as an in-land region of the KwaZulu-Natal province. Therefore, provided that the data were collected in low-lying terrains it is inclined to record high wind speeds as the daily wind speed for that region is already high. Given the high wind speeds experienced by a moving vehicle, there is a need for a system to control the airflow fed into the wind turbine, provided that the wind turbine generally has a cut-out wind speed of 25 m $s^{-1}$. These results were comparable to the wind speed data collected by Gururaj and Vasudha (2019) for a moving vehicle over five days. Gururaj and Vasudha (2019) reported an average apparent wind speed of 15.19 m $s^{-1}$ for a vehicle speed of 60 km $h^{-1}$ and an apparent wind speed of 21.74 m $s^{-1}$ for a vehicle speed of 80 km $h^{-1}$ which falls within the range of apparent wind speed specified in Table 5.

For theoretical calculations, the undisturbed wind speed was determined using the apparent wind speed equation, which is dependent on the daily airspeed, vehicle travelling speed and the true pointing angle. Table 6 shows the computed wind speed at different vehicle travelling speeds and an air speed which is assumed to remain constant at 1.944 m $s^{-1}$.

The outcomes from both the direct wind speed measurements and theoretical wind speed calculations are in agreement and this indicates that either method can be used to attain the apparent/undisturbed wind speed. In this study, the incoming wind speed is used in conjunction with the vehicle speed since the apparent wind speed is highly influenced by the vehicle speed. For this study

**Table 7** External and internal wind speeds at different louvre opening levels

| Louvre opening level | External wind speed (m $s^{-1}$) | Internal wind speed (m $s^{-1}$) |
|---|---|---|
| 0 (closed) | 7.2–14.2 | 0.2–0.3 |
| | 15.0–26.5 | 0.2–0.3 |
| | 27.0–35.1 | 0.2–0.3 |
| 1 | 7.2–14.2 | 2.9–9.4 |
| | 15.0–26.5 | 13.9–19.9 |
| | 27.0–35.1 | 17.5–27.0 |
| 2 (fully open) | 7.2–14.2 | 6.5–11.3 |
| | 15.0–26.5 | 14.4–25.9 |
| | 27.0–35.1 | 21.5–35.1 |

which is based on transportation, it is easy to relate the incoming wind speed to vehicle speed and therefore the incoming wind speed that is fed into the wind turbine is represented by the vehicle travelling speed.

Table 7 presents the external and internal wind speed at three louvre opening levels including the close louvre setting. These opening levels of the louvre mechanism were determined with the help of a vacuum blower to calibrate the internal wind speed simulating the external wind speeds that are fed into the wind turbine rotor. This was done to assist control the incoming wind speed and ensure that the turbine blades did not break due to high wind speeds. At opening level 0, the internal wind speed recorded was 0.2–0.3 m $s^{-1}$ for every wind speed range. This is because the louvre slats were shut and did not permit airflow, which is good in the case when the wind turbine is not required to generate power because the battery is full or for any other reason. The highest internal wind speed obtained at opening level 1 ranged between 17.5 and 27.0 m $s^{-1}$ from an external wind speed range of 27.0–35.1 m $s^{-1}$. On average it was found that the louvre mechanism can reduce the external wind speed by 5 m $s^{-1}$ to obtain the required internal wind speed, that is when operating at opening level 1. At the 2nd opening level, the highest recorded internal wind speed was 21.5–35.1 m $s^{-1}$ from an external wind speed of 27.0–35.1 m $s^{-1}$. Opening level 2 can obtain an average reduction of wind speed by 2.4 m $s^{-1}$. This means there is less airflow reduction in terms of wind speed at opening level 1. Opening level 2 is great when there is a need to drastically reduce the incoming wind speed and opening level 2 is good for a minor reduction of the incoming wind speed.

#### Power output of the wind turbine

Figure 10 shows the power output at different vehicle speeds. From the graph it can be seen that vehicle speed has a significant effect or impact ($p < 0.001$) on the power output of the wind turbine. The average power output ranged from 71.4, 105 to 129.4 W for a vehicle speed of 60. 80 and 100 km $h^{-1}$, respectively, averaged for both louvre opening levels 1 and 2. The low averages presented are due to low readings of power produced when the wind turbine was operating at louvre opening level 1. The authors observed that the power output values obtained from the vehicle speeds of 80 and 100 km $h^{-1}$ are close in terms of magnitude. This proves that high wind speed accounts for the low swept area (0.283 $m^2$) of the wind turbine rotor to produce more power output. The wide range of the incoming wind speed values that affect the wind turbine energy generation is represented

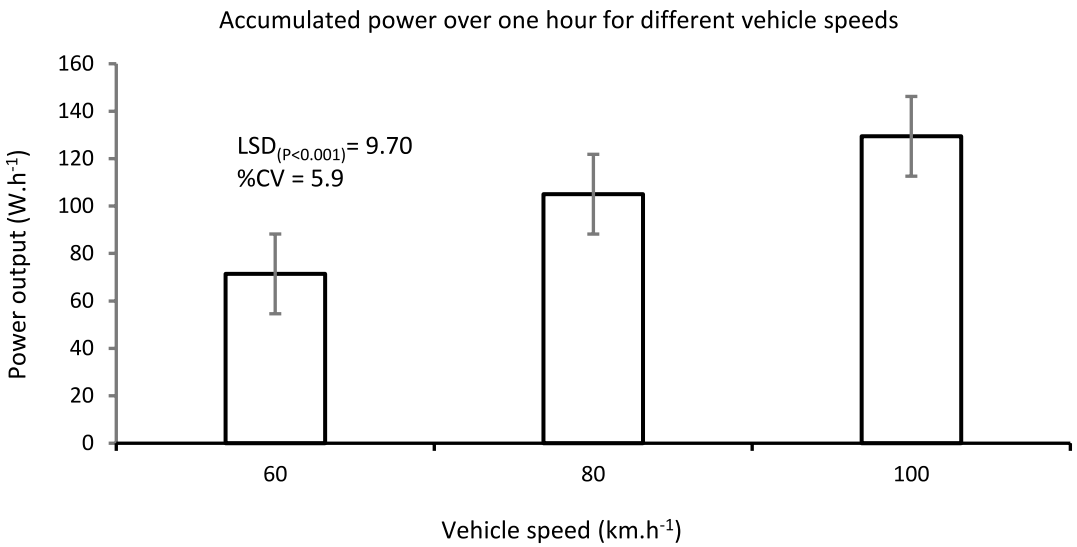


**Fig. 10** Effect of vehicle speed on accumulated power

by the vehicle travelling speed since the apparent wind speed harnessed and used for power generation is highly dependent on the travelling speed.

The cut-in wind speed was observed at 4 m $s^{-1}$ while the rated wind speed was observed at 17.5 m $s^{-1}$. No cut-out wind speed was observed although the highest wind speed observed was at 33 m $s^{-1}$. These observations are comparable to the study done by Barroso Montes (2011) who observed a cut-in and cut-out wind speed of 5 and 25 m $s^{-1}$, respectively, and Hirahara et al. (2005) who observed a cut-in wind speed of 3.6 m $s^{-1}$, a rated wind speed of 12 m $s^{-1}$ and a survival wind speed of 45 m $s^{-1}$. Also, the findings of this study are relatable to the results found by Salih et al. (2012) who observed a cut-in wind speed of 4 m $s^{-1}$, a rated wind speed of 12 m $s^{-1}$ and a cut-out wind speed of 25 m $s^{-1}$. No damage was observed on the overall wind turbine and the blades even though the wind turbine also operated at high wind speeds of more than 25 m $s^{-1}$ which is the common cut-out wind speed value for most research studies.

Figure 11 shows the effect of controlling the airflow that is fed into the wind turbine through the louvre mechanism. The average power output is 73.9 and 129.9 W for louvre opening levels 1 and 2, respectively. This clearly shows that the opening level of the louvre mechanism has a significant effect ($p < 0.001$) on the amount of power generated by the wind turbine. The power output achieved from this study using different wind speeds is far greater than depicted in this graph. This is because each of these values is an average for all vehicle travelling speeds. The airflow in this case did not require interference because high wind speeds were required to generate high-power output. Although still, the louvre mechanism design can be helpful in extreme wind conditions to control the incoming wind speed as well as protect the rotor and generator. Ultimately, this mechanism will enable the wind turbine to operate and generate electrical energy in strong wind conditions. No loud and intolerable noise was perceived during the testing that could be an inconvenience to other drivers on the road.

Figure 12 shows the accumulated power observed at different durations for an hour. It can be seen that the accumulated power is directly related to time. There is a definite increase in the accumulated power output with growing time ($p < 0.001$) although this can be affected by the change in topography and terrains as previously discussed in section Incoming wind speed determination. This simply shows that the amount of power generated by the wind turbine continuously increases with time as it accumulates.

Figure 13 depicts the accumulated power output subjected to different louvre opening levels and vehicle travelling speeds. The accumulated power of 113.4, 159.6 and 210.0 W per hour were observed for 60, 80 and 100 km $h^{-1}$, respectively, on louvre opening level 1. On louvre opening level 2, the power output observed in an hour was 142.8, 268.8 and 294.0 W for a wind speed of 60, 80, and 100 km $h^{-1}$, respectively. The graph on display shows that the vehicle speed of 100 km $h^{-1}$ achieves a

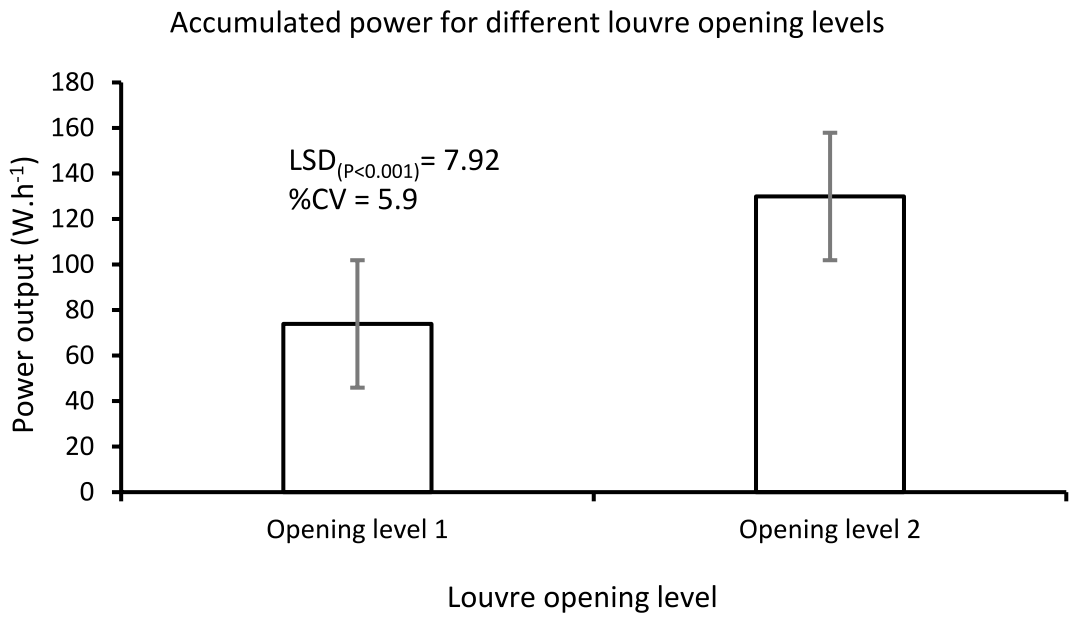


**Fig. 11** Effect of louvre opening level on the accumulated power of the small wind turbine

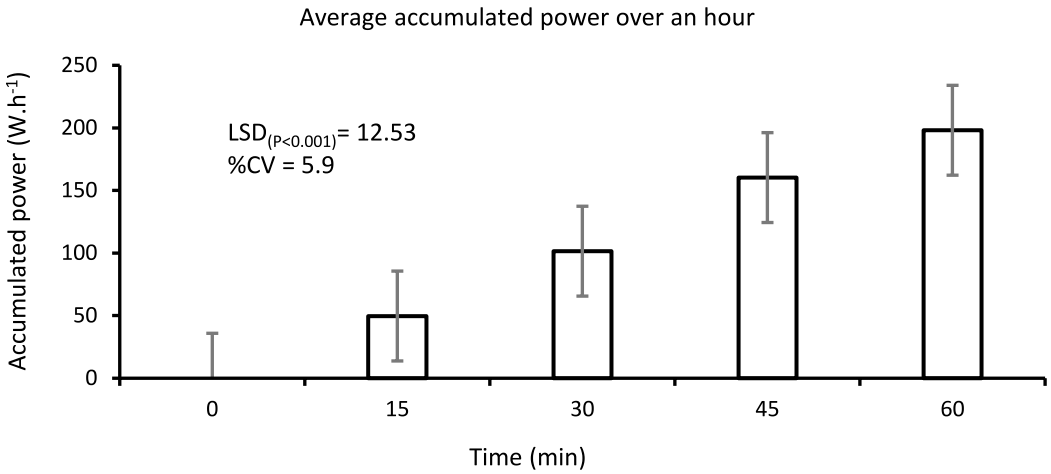


**Fig. 12** Accumulated power of the small wind turbine over one-hour duration

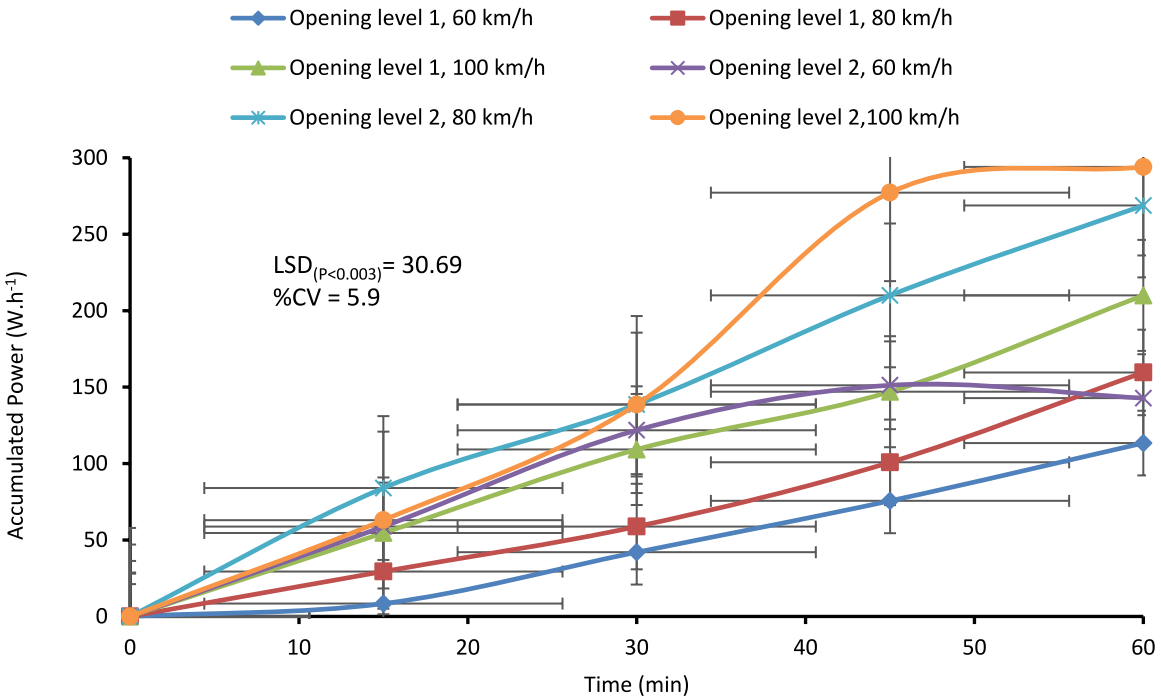


**Fig. 13** Accumulated power over time for different vehicle speeds and louvre opening level of the wind turbine

high-power output compared to the other vehicle speeds of 60 and 80 km $h^{-1}$. An increase in vehicle speed implies an increase in the wind speed. Travelling speeds above 100 km $h^{-1}$ were not investigated due to the 100 km $h^{-1}$ speed restrictions placed on vehicles carrying goods with gross vehicle mass between 3 500 and 9 000 kg.

Figures 10, 11, 12 and 13 show the effect of vehicle speed, louvre opening level, and time on the average accumulated power generated by a small wind turbine with a rotor diameter of 0.6 m. The power output of the 600-W PMSG ranged between 113.4 and 294 W per hour for a vehicle speed of 60, 80 and 100 km $h^{-1}$ (16.67, 22.22 and 27.78 m $s^{-1}$). The findings obtained in this study are comparable to the results obtained by Ozgener (2006) who reported a power output of 616 W for a 1.5 kW wind turbine generator at 7.5 m $s^{-1}$ with a rotor diameter of 3 m which translates to 49% and 41% efficiencies, respectively, for this study's and Ozgener (2006) findings. Tahir et al. (2019) also conducted a wind turbine study which produced 478.5 W for a 600-W permanent magnet

generator operating at 10 m $s^{-1}$ and a rotor diameter of 0.65 m and achieved 79% efficiency. The difference in the findings of this study may be attributed to the small size of the rotor diameter, the material used for the blade design (PVC) and the changing topography of surrounding areas along the road during testing. Another important factor that possibly affects the performance of the wind turbine is the torque or ease of rotation of the generator shaft which in this case moved well but felt tight and strained along its operation. Although given these constraints, the generated power output can still meet the power requirement for half the expected time of an hour. This may suggest the need for a bigger generator size of 1200 W to meet the power requirement of 600 W. The results obtained by Ozgener (2006) also suggest that an electric generator two or three times the size of the system's (cooling technology) power requirement should be acquired. The power from the wind turbine is then stored in the battery. The charging capacity is measured through the voltage state of charge. The inverter then steps up the voltage in the battery from 12 to 230 V, which then allows the wind turbine to provide the current that is required to meet the power requirement of two fans and a water pump.

Based on the results it is clear that a substitute can be made between the wind speed and the rotor diameter. Authors such as Ozgener (2006), Salih et al. (2012) and Tahir et al. (2019) performed studies which analysed wind turbines with low wind speeds and large rotor sizes. Salih et al. (2012) designed a 700 W wind turbine with a rotor diameter of 1.6 m which produced a 600-W electrical power at 12 m $s^{-1}$. In this study, the 600-W wind turbine was designed with a high design wind speed (16.8–19.0 m $s^{-1}$) and a small rotor diameter (0.6 m). This proves the initial prediction that the wind speed accounts for the small nature of the rotor in some way to produce electric power for a wind turbine. In this study, it was observed that in traffic areas, the power output was low due to low travelling speeds resulting in low incoming wind speed being created. Thus, the battery must be used in this case. During the testing, it was observed that the apparent wind turbine had no physical impact on the stability of the moving vehicle, although the wind turbine may have some slightly negative impact on the fuel efficiency and result in some aerodynamic drag because of the added weight. There is no need to prime or kickstart the generator. The wind turbine only needs less than 10 s to start operating if the vehicle was stationary.

### *Power coefficient of the wind turbine*

Figure 14 shows the power coefficient computed for the different power outputs subjected to different louvre

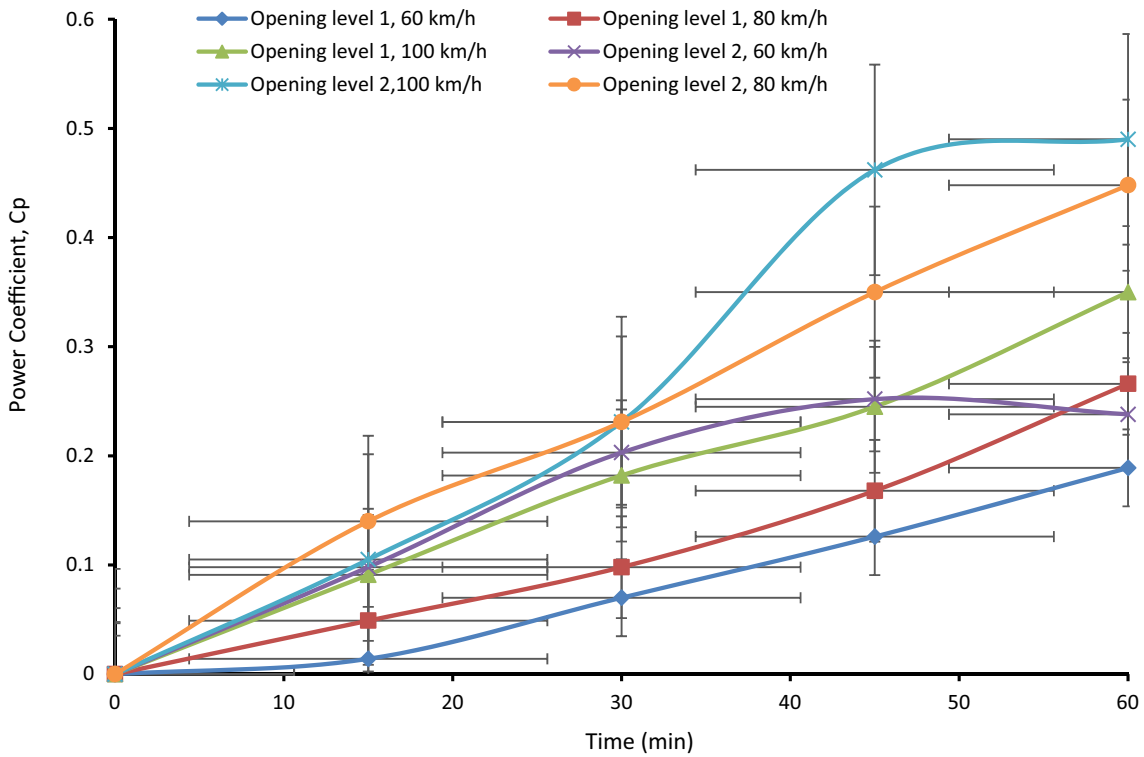


**Fig. 14** Power coefficient for different vehicle speeds

opening levels and vehicle speeds for a duration of one hour. The power coefficient ranged between 0.19 and 0.35 for louvre opening level 1 and 0.24–0.49 for louvre opening level 2. From Fig. 14 it can be seen that the maximum power coefficient of 0.49 is achieved at a vehicle speed of 100 km $h^{-1}$ and louvre opening level 2. These results are credible since the maximum power coefficient achieved in this study is close but does not exceed the Betz limit at 0.59. The findings are comparable to the studies performed by authors such as Ozgener (2006) (0.35), and Muhsen et al. (2019) (0.4–0.445). This power coefficient of 0.49 is comparable to the maximum power coefficient of 0.44 obtained by QBlade modelling.

Figure 15 shows how the power coefficient is been affected by the vehicle speed. The results prove that the power coefficient improves with increasing vehicle speed. In this particular case, the louvre opening level 2 also had an effect on the power. The maximum power coefficient obtained in this study is 0.49. Salih et al. (2012) evaluated the power output of a 600-W wind turbine against the wind speed and found that the power output increases with an increasing speed up until the rated wind speed where it stabilises and produces the same amount of power until the cut-out wind speed. It is recommended to use to vehicle speed of 80–100 km $h^{-1}$ when transporting fresh produce with this wind turbine. Furthermore, it is suggested to lower the louvre opening level when there are strong wind conditions to prevent blades from breakage and still be able to generate electrical energy which is much needed by the cooling technology.

## Conclusion

The aim of the study was to design and develop a low-cost, portable, small wind turbine prototype that can be used to power a mobile evaporative cooling technology, particularly an ECS unit. The small wind turbine incorporated a louvre mechanism to assist in controlling the wind speed at the front of the rotor. The outcome of this study revealed that the power output of the small wind turbine (0.6 m ∅) is highly influenced by vehicle speed and the louvre opening level which make up for the small size of the rotor. For a small wind turbine, with a small rotor diameter, the surface area of the blades must be increased in terms of the chord lengths in order to harness the desired power output. The highest average power output achieved was 294.0 W at 100 km $h^{-1}$ for louvre opening level 2. From the rotor, the 230 VAC step-up power inverter was used to step the voltage to power the 600-W load, hence, based on the operation of the system, the wind turbine prototype design can be adjudged to be successful. Although the power generated may only cover half an hour, hence, this wind turbine system can be utilised as a hybrid solution with a diesel engine or solar. It can be used as backup power as well as a hybrid system at this stage of development. The maximum power coefficient obtained from this study was 0.49 which is a good indication that the system functions efficiently provided that the maximum power coefficient that can be attained by any wind turbine is typically 0.59, known as the Betz limit. Given these results, it must be understood that this research was a success although it serves as exploratory work which requires further testing in

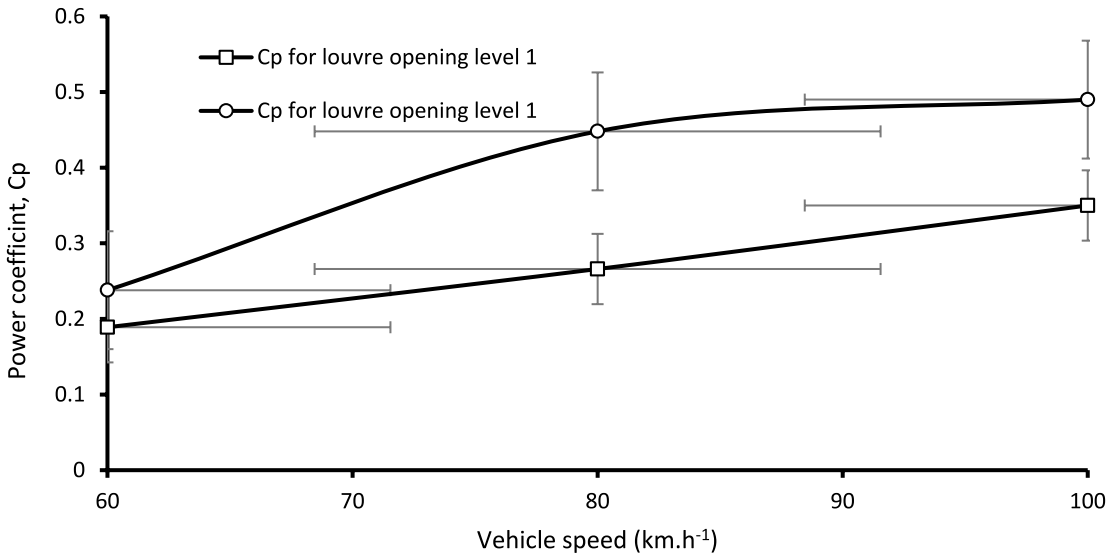


**Fig. 15** Power coefficient for different vehicle speeds

terms of the chosen material strength, endurance and power generation in comparison to other materials.

## Recommendations

Based on the findings of this study, the following recommendations were suggested:

1. Investigate the aerodynamic effect of the wind load on the mounted wind turbine and the vehicle.
2. Perform the fatigue analysis of the blades to determine the life span of the PVC blades.
3. Develop a trailed ECS unit powered by the wind turbine instead of a portable, bakkie-mounted ECS unit.
4. Investigate the possible aerodynamic/drag effect of the wind turbine on the overall performance of the vehicle and fuel efficiency.
5. Add a wire mesh or net at the back of the wind turbine as a safety measure to ensure that in the case of a blade breakage or any other component, it does not pose a risk to the rear vehicles coming after which can potentially cause accidents.
6. Automate the louvre mechanism to improve the ease of operation with the assistance of wind speed sensors.
7. A comparison study between the PVC blades and other blade materials should be conducted in terms of power generation and material strength.

### Abbreviations

| | |
|---|---|
| PHLs | Postharvest losses |
| FVs | Fruit and vegetables |
| BEM | Blade element momentum |

### List of symbols

| | |
|---|---|
| A | Apparent wind speed (m $s^{-1}$) |
| V | Vehicle speed (m $s^{-1}$) |
| W | Wind velocity, and is the true pointing angle (°) |
| $P_A$ | Accumulated/ aerodynamic power ((W $h^{-1}$) |
| CC | Capacity charge (%) |
| E | Electrical energy of the battery (Wh) |
| $C_p$ | Power coefficient |
| $P_T$ | Total power rating of the wind turbine (W $h^{-1}$) |

### Acknowledgements

We are grateful to the Agricultural Engineering workshop technical staff for the assistance in the development of the prototype.

### Author contributions

The corresponding author, Perm Mthethwa designed and developed the wind turbine prototype, conducted the wind turbine tests, analysed and interpreted the obtained results and wrote the manuscript. Tilahun S. Workneh and Alaika Kassim conceived and designed the wind turbine, supervised the testing and read and approved the manuscript.

### Funding

This work was funded by Workneh JW Nelson and Seyoum UKZN scholarship.

### Availability of data and materials

The datasets used and/or analysed during the current study are available from the corresponding author on reasonable request.

## Declarations

### Competing interests

The authors declare that they have no competing interests.

Received: 5 December 2023 Accepted: 2 June 2024
Published online: 13 June 2024

### References

Akbari, V., Naghashzadegan, M., Kouhikamali, R., Afsharpanah, F., & Yaïci, W. (2022). Multi-objective optimization and optimal airfoil blade selection for a small horizontal-axis wind turbine (HAWT) for application in regions with various wind potential. *Machines, 10*(8), 687. https://doi.org/10.3390/machines10080687

Barroso Montes, M. (2011). Optimal control of wind turbines in strong wind conditions.

Bisoyi, S.K., Jarial, R., and Gupta, R. (2013). Modeling and control of variable speed wind turbine equipped with PMSG. *International Journal of Emerging Technologies in Computational and Applied Sciences, 6*(1), 56–62, https://doi.org/10.14741/ijcet/spl.2.2014.78.

Bracco, G., & Razzetti, D. (2022). *Aerodynamic design of a micro wind turbine and performance analysis with QBlade*. Turin: Master of Science, Mechanical Engineering, Polytechnic University of Turin. https://doi.org/10.1007/978-94-007-5968-8_15

Ceruti, A. (2019). Meta-heuristic multidisciplinary design optimization of wind turbine blades obtained from circular pipes. *Engineering with Computers, 35*, 363–379. https://doi.org/10.1007/s00366-018-0604-8

Cherono, K., & Workneh, T. (2020). The efficacy of postharvest biocontrol treatments in controlling spoilage of tomato fruit in South African commercial supply chains. *Journal of Engineering in Agriculture and the Environment, 5*(2), 19–25. https://doi.org/10.37017/jeae-volume5-no2.2019-4

Chong, C., Rigit, A., and Ali, I. (2021). Wind turbine modelling and simulation using Matlab/SIMULINK, in IOP Conference Series: Materials Science and Engineering, Kuching, Malaysia, 27–28 October 2020,1101, 012034, https://doi.org/10.1088/1757-899x/1101/1/012034.

Dew, R., Seal, C.J., and Brandt, K. (2014). Effects of temperature conditions during transport and storage on tomato fruit quality, in Proceedings of the XXIX International Horticultural Congress on Horticulture: Sustaining Lives, Livelihoods and Landscapes (IHC2014), Brisbane, Australia, August 2014. https://doi.org/10.17660/ActaHortic.2016.1120.48.

Elik, A., Yanik, D. K., Istanbullu, Y., Guzelsoy, N. A., Yavuz, A., & Gogus, F. (2019). Strategies to reduce post-harvest losses for fruits and vegetables. *International Journal of Scientific and Technological Research Strategies, 5*(3), 29–39. https://doi.org/10.7176/jstr/5-3-04

Evans, S., Bradney, D., & Clausen, P. (2018). Development and experimental verification of a 5 kW small wind turbine aeroelastic model. *Journal of Wind Engineering and Industrial Aerodynamics, 181*(2018), 104–111. https://doi.org/10.1016/j.jweia.2018.08.011

Garmode, R. K., Gaval, V. R., Kale, S. A., & Nikhade, S. D. (2022). Comprehensive evaluation of materials for small wind turbine blades using various MCDM techniques. *International Journal of Renewable Energy Research, 12*(2), 981–992. https://doi.org/10.20508/ijrer.v12i2.12992.g8481

Hirahara, H., Hossain, M. Z., Kawahashi, M., & Nonomura, Y. (2005). Testing basic performance of a very small wind turbine designed for multi-purposes. *Renewable Energy, 30*(2), 1279–1297. https://doi.org/10.1016/j.renene.2004.10.009

Hossain, M. F. (2020). Application of wind energy into the transportation sector. *International Journal of Precision Engineering and Manufacturing-Green Technology, 8*, 1225–1237. https://doi.org/10.1007/s40684-020-00235-1

Kuhudzai, R.J. (2022). South Africa's Shoprite Group Now Has 1041 Trailers With Solar-Powered Refrigeration For Its Fleet. Clean Technica. https://cleantechnica.com/2022/11/30/the-shoprite-group-becomes-the-first-south-african-retailer-to-pilot-a-heavy-duty-electric-truck/.

Louw, A., & Jordaan, D. (2016). Supply chain risks and smallholder fresh produce farmers in the Gauteng province of South Africa. *Southern African Business Review, 20*(2016), 286–312. https://doi.org/10.25159/1998-8125/6051

Mansuri, S.M., Sharma, P., and Samuel, D. (2016). Solar powered evaporative cooled storage structure for storage of fruits and vegetables. *Indian Journal of Agricultural Sciences*, *86*(7), 916–22. https://epubs.icar.org.in/ejournal/index.php/IJAgS/article/view/59825/24627.

Mthethwa, P., Workneh, T. S., & Kassim, A. (2022). Small wind turbine blade optimisation and design using QBlade for integration into a low-cost fresh produce preservation technology. *Acta Horticulturae, 1349*(2022), 417–426. https://doi.org/10.17660/ActaHortic.2022.1349.56

Mthethwa, P., Workneh, T. S., & Kassim, A. (2023). Renewable energy integration into a low-cost evaporative cooling system for fresh produce storage. In T. S. Workneh (Ed.), *Engineering principles, modeling and economics of evaporative coolers* (pp. 219–243). Amsterdam: Elsevier. https://doi.org/10.1016/B978-0-323-90039-3.00008-6

Muhsen, H., Al-Kouz, W., & Khan, W. (2019). Small wind turbine blade design and optimization. *Symmetry, 12*(1), 18. https://doi.org/10.3390/sym12010018

Murthy, D. S., Gajanana, T., Sudha, M., & Dakshinamoorthy, V. (2009). Marketing and post-harvest losses in fruits: Its implications on availability and economy. *Indian Journal of Agricultural Economics*. https://doi.org/10.22004/ag.econ.204629

Ozgener, O. (2006). A small wind turbine system (SWTS) application and its performance analysis. *Energy Conversion and Management, 47*(11–27), 1326–1337. https://doi.org/10.1016/j.enconman.2005.08.014

Panja, P. and Ganguly, A. (2019). Modelling and analysis of a hybrid solar thermal and biomass driven vapor absorption refrigeration system for cold storage purpose, in Proceedings of fifth international congress on engineering and technology (ICET2019), Pune, India, March 2019, https://doi.org/10.36375/prepare_u.a26.

Rossetti, A., Marinetti, S., Artuso, P., Fabris, F., and Minetto, S. (2022). Implementation of a solar aided refrigration unit for refrigerated trucks employing photovoltaic generators. *Energy Reports, 8*, 7789–7799. https://doi.org/10.1016/j.egyr.2022.05.284.

Saidi, Y., Mezouar, A., Miloud, Y., and Benmahdjoub, M. A. (2018). A robust control strategy for three phase voltage t source PWM rectifier connected to a PMSG wind energy conversion system, in 2018 International Conference on Electrical Sciences and Technologies in Maghreb (CISTEM), 2018: IEEE, 1–6, https://doi.org/10.1109/cistem.2018.8613359.

Salih, S. M., Taha, M. Q., & Alawsaj, M. K. (2012). Performance analysis of wind turbine systems under different parameters effect. *International Journal of Energy and Environment, 3*(6), 895–904.

Schubel, P.J. and Crossley, R.J. (2012). Wind turbine blade design. *Energies, 5*(9), 3425–3449. https://doi.org/10.1260/0309-524X.36.4.365.

Shoaib, M., Siddiqui, I., Rehman, S., Khan, S., & Alhems, L. M. (2019). Assessment of wind energy potential using wind energy conversion system. *Journal of Cleaner Production, 216*, 346–360. https://doi.org/10.1016/j.jclepro.2019.01.128

Sibanda, S., & Workneh, T. S. (2020a). Performance evaluation of an indirect air cooling system combined with evaporative cooling. *Heliyon, 6*(1), e03286. https://doi.org/10.1016/j.heliyon.2020

Sibanda, S., & Workneh, T. S. (2020b). Potential causes of postharvest losses, low-cost cooling technology for fresh produce farmers in Sub-Sahara Africa. *African Journal of Agricultural Research, 16*(5), 553–566. https://doi.org/10.5897/ajar

Tahir, M. H., Malik, A., Saeed, M. A., Zaffar, N., Adeel, H. M., and Amjad, H. M. S. (2019). Experimental Performance Evaluation of 600 W Small Wind Turbine to Overcome Energy Crisis in Pakistan.

Telle, J. S., Schlüters, S., Schönfeldt, P., Hanke, B., von Maydell, K., & Agert, C. (2022). The optimized integration of temperature-controlled transports into distributed sector-integrated energy systems. *Energy Conversion and Management, 269*, 116148. https://doi.org/10.1016/j.enconman.2022.116148

Van Duin, J. R., Geerlings, H. H., Verbraeck, A. A., & Nafde, T. T. (2018). Cooling down: A simulation approach to reduce energy peaks of reefers at terminals. *Journal of Cleaner Production, 193*, 72–86. https://doi.org/10.1016/j.jclepro.2018.04.258

Wahyudi, B., Faizin, A., Setiawan, A., Susilo, S. H., & Wicaksono, H. (2022). Simulation study of horizontal axis wind turbine using PVC pipe propeller with elbow tip. *EUREKA Physics and Engineering, 5*, 67–76. https://doi.org/10.21303/2461-4262.2022.002550

Wood, D. (2011). Small wind turbines, in Advances in wind energy conversion technology: Springer, 195–211, https://doi.org/10.1007/978-3-540-88258-9

Zhang, Q., He, J., Xu, Y., Hong, Z., Chen, Y., & Strunz, K. (2021). Average-value modeling of direct-driven PMSG-based wind energy conversion systems. *IEEE Transactions on Energy Conversion, 37*, 264–273. https://doi.org/10.1109/tec.2021.3095486

## Publisher's Note